# Mechanical identities of RNA and DNA double helices unveiled at the single-molecule level

Elías Herrero-Galán[†,‡], Maria Eugenia Fuentes-Perez[‡], Carolina Carrasco[‡], José M. Valpuesta[‡], José L. Carrascosa[†,‡,§], Fernando Moreno-Herrero[*,‡], J. Ricardo Arias-Gonzalez[*,†,‡,§].

[†]Instituto Madrileño de Estudios Avanzados en Nanociencia (IMDEA Nanociencia), Cantoblanco, 28049 Madrid, Spain. [‡]Department of Macromolecular Structure, Centro Nacional de Biotecnología (CNB-CSIC), Cantoblanco, 28049 Madrid, Spain. [§]CNB-CSIC-IMDEA Nanociencia Associated Unit "Unidad de Nanobiotecnología".

Supporting Information Placeholder

**ABSTRACT:** Double-stranded (ds) RNA is the genetic material of a variety of viruses and has been recently recognized as a relevant molecule in cells for its regulatory role. Despite the elastic response of dsDNA has been thoroughly characterized in recent years in single-molecule stretching experiments, an equivalent study with dsRNA is still lacking. Here, we have engineered long dsRNA molecules for their individual characterization contrasting information with dsDNA molecules of the same sequence. It is known that dsRNA is an A-form molecule unlike dsDNA which exhibits B-form in physiological conditions. These structural types are distinguished at the single-molecule level with Atomic Force Microscopy (AFM) and are the basis to understand their different elastic response. Force-extension curves of dsRNA with optical and magnetic tweezers manifest two main regimes of elasticity, an entropic regime whose end is marked by the A-form contour-length and an intrinsic regime that ends in a low-cooperative overstretching transition in which the molecule extends to 1.7 times its A-form contour-length. DsRNA does not switch between the A and B conformations in the presence of force. Finally, dsRNA presents both a lower stretch modulus and overstretching transition force than dsDNA, whereas the electrostatic and intrinsic contributions to the persistence length are larger.

## INTRODUCTION

Two chemically different molecules to store information are found in nature, both characterized by their ability to form complementary double-helix chains. DsDNA is the selected molecule by most organisms although dsRNA keeps an identical capability for this role since it is equally based on a four-letter alphabet. However, the existence of the latter as an information carrier is confined to viral genomes. Over the past few years, dsRNA has emerged as a far more relevant molecule than previously expected. The discovery of RNA interference has demonstrated that dsRNA molecules play a key role in the life cycle of a cell[1-3]. Interest in RNA nanotechnology has also increased as recognition of its potential applications in nanomedicine has grown[4,5].

The structure of double-stranded nucleic acids has been long investigated in an effort to get insights into their functions, as well as to understand the molecular basis of the way in which different proteins carry out their replication, repair and transcription. These studies have revealed the existence of distinctive double-helix states in physiological conditions, namely, the A and the B forms for dsRNA and dsDNA, respectively[6,7]. Mechanical characterizations of dsDNA at the single-molecule level in a broad palette of conditions have also been performed[8], including those which stabilize the so-called A-DNA[9-11]. These studies have opened new avenues of research on nucleic acid-binding proteins, especially to understand from a dynamic point of view the intimate link between information processing by such molecular machines and the mechanical properties of their respective substrates[8,12-14].

The intrinsic difficulty of working with RNA, due to the labile nature of single-stranded (ss) RNA intermediates and the lack of restriction enzymes working on these substrates, has hindered the development of the needed tools to study the mechanical properties of dsRNA[15]. Former experiments regarding single-molecule mechanical measurements at zero or low force values have been performed[16], but no data is available yet at high forces, where information on the stretch modulus and the overstretching behavior is obtained. Likewise, no direct comparison between dsRNA and dsDNA has been performed in the same study, an evaluation which is required to rigorously establish the elastic identities that stem from their different chemical nature and subsequent structural states.

In this work, we have engineered long dsRNA molecules for their individual characterization by means of optical tweezers (OT) and magnetic tweezers (MT)[13,17]. We present complete force-extension curves of dsRNA reaching the overstretching transition and compare the results with the behavior of equivalent dsDNA molecules. The discussion on the structure-elasticity relationship is sup-

ported by AFM images which in situ discriminate both substrates at the single-molecule level and by a bulk biophysical analysis that includes circular dichroism (CD) and differential scanning calorimetry (DSC). Our study represents a single-molecule platform not only to assess the elastic response of dsRNA but also to understand how chemically different nucleotides lead to similar information carriers with distinctive mechanical response.

## EXPERIMENTAL SECTION

**Synthesis of dsRNA molecules with multilabeled ends**. Long dsRNA molecules with multilabeled ends for OT measurements were synthesized according to the protocol described by Dekker et al.[15], with slight modifications in order to increase yield and ligation efficiency for single-molecule manipulation purposes. Briefly, desired overhangs were introduced together with the T7 RNA polymerase promoter in λ phage [30286, 34286] template DNA by PCR. Afterwards, in vitro transcription (3 h, 42ºC) using the commercial HiScribe kit (New England Biolabs) gave rise to two complementary 4-kbp single strands of RNA with a few non-complementary nucleotides at their 5' ends. After addition of EDTA to a 30 mM final concentration, both strands were subsequently hybridized by heating 1 h at 65ºC and slowly cooling down to room temperature at a 1.2ºC/5 min rate, to form 4-kbp dsRNA molecules with controlled single-stranded overhangs. Multilabeled ~0.5-kbp dsRNA fragments were generated following a similar protocol in presence of digoxigenin-11-UTP or biotin-16-UTP (1-4 molar units) during the transcription step. The sequence [23137, 23630] of λ DNA was used this time as a template, complementary overhangs to those of the main 4-kbp molecule being added only at one end per dsRNA fragment. Transcription products were then treated with ten units of RNase-free DNase I (Roche) and, prior to ligation, 5'-triphosphates were replaced by 5'-monophosphates using the KinaseMax Kit (Ambion). The 4-kbp dsRNA main molecule was finally ligated to the 0.5-kbp multilabeled fragments with T4 RNA ligase 2 (New England Biolabs) by incubation at 16ºC during 16 h. Every step was followed by purification with the RNeasy MinElute Cleanup Kit (Qiagen). DNA and RNA substrates were stored in TE buffer (10 mM Tris-HCl, 1 mM EDTA, pH 8.0). Figure 1A shows the average Guanine-Cytosine (GC)-content of the sequence employed.

**Synthesis of dsDNA control molecules with multilabeled ends**. DsDNA control molecules for OT measurements, with the same length and sequence as the previously described dsRNA ones, were generated as follows. Two different restriction sites, KpnI and SacI, absent within the λ [30286, 34286] sequence, were introduced one at each end of the template DNA by site directed mutagenesis. In the same way, the sequence [23137, 23630] was mutated to include either a KpnI or a SacI restriction site at one end, each PCR product being synthesized in presence of biotin-16-dUTP or digoxigenin-11-dUTP, respectively. Further digestion and ligation of complementary fragments with T4 DNA ligase (Roche) at 16ºC during 16 h gave rise to 4-kbp dsDNA molecules with two 0.5-kbp ends differently labeled, as it was the case for dsRNA molecules used in this study. DsDNA and dsRNA molecules thus have exactly the same sequence except for five nucleotides on each overhang. These differences do not affect the stretching measurements, as they are performed over the main 4-kbp molecular fragment, the multilabeled ends functioning only as linkages to the polystyrene beads to allow manipulation.

For control experiments aimed to test the influence of GC content in the relative melting behavior of both nucleic acids, three additional 4-kbp dsRNA molecules and their corresponding dsDNA counterparts with the same length and sequence were prepared as described above from fragments [3686, 7686] of plasmid pSP73-JY0 (35% GC), [26000, 30000] of λ DNA (41% GC) and [3100, 7100] of λ DNA (60% GC).

**Circular dichroism**. Circular dichroism (CD) spectra of both dsRNA and dsDNA molecules were registered in 10 mM Tris buffer, with 150 mM NaCl, 1 mM EDTA at pH 8.0, on a Jasco 715 spectropolarimeter, equipped with a thermostated cell holder and a Neslab-111 circulating water bath. The instrument was calibrated with (+)-10 camphorsulphonic acid. Spectra were collected at 20ºC and 20 nm/min using a circular quartz cuvette of 0.1-cm optical path. Mean residue weight ellipticities are expressed as degree·cm$^{2}$·dmol$^{-1}$. Melting transitions were detected as a decrease in CD signal at 260 nm for dsRNA and at 275 nm in the case of dsDNA using a 1-cm optical path cuvette in a JASCO 800 spectropolarimeter equipped with a Peltier Temperature Control System. Experiments were performed in 25-mM phosphate buffer with 150 mM NaCl and 1 mM EDTA (pH 8.0), and temperature was increased at a 60ºC/h rate.

**Differential scanning calorimetry**. Differential Scanning Calorimetry (DSC) profiles of 4-kbp dsRNA and dsDNA control molecules, in the 20-100ºC range, were registered on a VP-DSC microcalorimeter (Microcal) at 60ºC/h scanning speed, either in 15 mM MOPS or 25 mM phosphate buffer, both with 150 mM NaCl and 1 mM EDTA at pH 8.0, with identical results. Several heating-cooling down cycles were performed in order to check the reversibility of the thermal transitions observed.

**Atomic Force Microscopy measurements**. A solution containing 0.25 nM dsDNA or dsRNA molecules and 25 mM Tris acetate (pH 7.5), 2.5 mM magnesium acetate, and 2.5 mM NiCl2 was deposited on freshly-cleaved mica. After 30 s, the mica surface was washed with 3 ml of MilliQ-filtered water and blown dry in a gentle stream of nitrogen gas. Images were obtained with an AFM from Nanotec Electronica S.L., operating in tapping mode in air, and using PointProbePlus tips (PPP-NCH, Nanosensors). Raw images were processed with WSxM freeware[18] applying the in-plane subtraction and flatten filter. The contour length of individual molecules was measured with the WSxM freeware and the persistence length was obtained following a procedure described elsewhere[9,19,20]. Sample deposition and data analysis was identical for both dsDNA and dsRNA.

**Optical Tweezers measurements**. Dual, counter-propagating laser beam (λ = 835 nm) OT were used to measure force from changes in light momentum flux[21]. Single molecules were tethered by opposite ends between two dielectric polystyrene microspheres: an α-digoxigenin-coated bead, optically trapped, and a streptavidin-coated bead, held by suction on top of a micropipette (Fig. 5 A, inset). Force on the studied molecule was exerted by moving the micropipette relative to the optically-trapped bead through a piezo-controlled stage, and its extension was measured from the distance between the centers of the beads. Stretch-relax cycles were performed at 500 nm/s. All experiments were carried out at room temperature (23 ± 1°C) in TE buffer at indicated salt concentrations.

**Magnetic Tweezers experiments.** The MT setup consists of a pair of magnets positioned over a flow cell on an inverted optical microscope[9,16]. Superparamagnetic beads, used as probes in the flow cell, were manipulated by an external force that pulls them towards the magnets. We used streptavidin-coated beads to bind the biotin-labelled end of the molecule, the digoxigenin-labelled end being bound to a glass surface covered by α-digoxigenin. Vertical positions (extensions) were determined from the diffraction rings of the tethered beads relative to beads affixed at the bottom of the flow cell. Force values were calculated using the Brownian motion method. Force-extension curves were obtained in TE buffer at indicated salt concentrations. Torsionally unconstrained single-molecule tethers were confirmed by rotating the magnets and observing no variation in height.

## RESULTS

To perform a strict comparison between dsDNA and dsRNA, we have used molecules of the same number of nucleotides and equivalent sequences. In this regard, 4-kbp long dsRNA molecules with multilabeled ends were obtained by in vitro transcription using the [30286, 34286] sequence of λ-phage DNA as a template (see Experimental Section). Figure 1A shows the average GC content of this λ-DNA region (slightly below 50%), which was also used to prepare multilabeled dsDNA control molecules.

**Bulk analysis**. Structural characterization of the substrates was performed by CD spectroscopy, a light-based technique which can discriminate structural states of a polymer in aqueous conditions. Figure 1B reveals the typical fingerprints of an A-form and a B-form nucleic acid for dsRNA and dsDNA molecules, respectively, in agreement with former literature[22,23]. The melting behavior is commonly described by DSC, in which the separation of the two strands as a function of temperature is signaled by a change in heat capacity ($\Delta C_p$). Figure 2A shows DSC profiles (normalized $\Delta C_p$ vs. temperature) as registered for both kinds of molecules used in this study. Thermograms showed a transition between 83°C and 100°C for dsRNA and a more cooperative one, between 85°C and 92°C, for dsDNA. The thermal transition of dsDNA is composed of several highly-cooperative

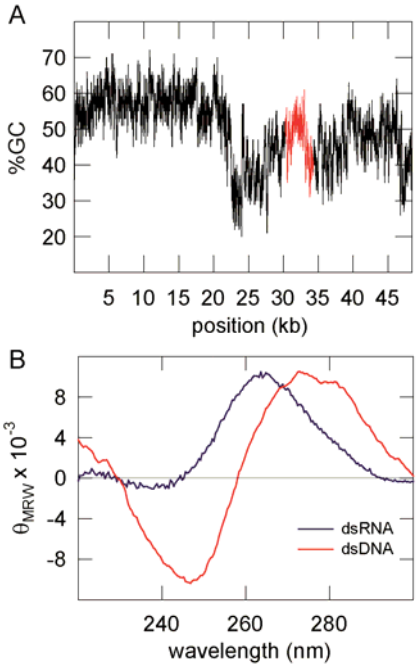


**Figure 1.** (A) GC content profile of λ DNA. The template [30286, 34286] sequence employed to prepare multilabeled dsRNA and dsDNA control molecules is highlighted in red. (B) Circular Dichroism spectra of dsRNA (blue) and dsDNA control molecules (red). $\theta_{MRW}$, mean residue weight ellipticity in units of degree·cm²·dmol⁻¹.

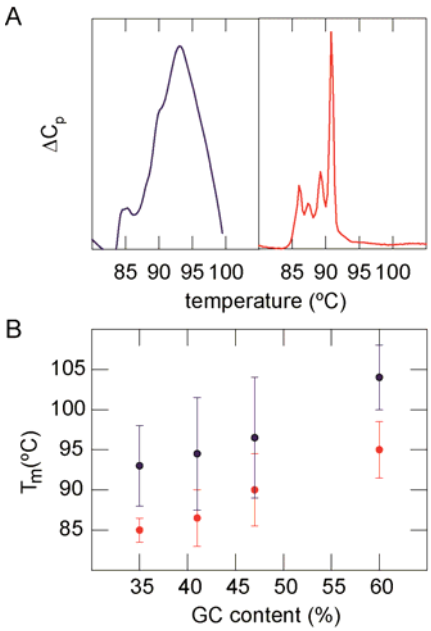


**Figure 2.** (A) Differential Scanning Calorimetry peaks obtained after thermal transition of dsRNA (blue) and dsDNA (red). Plots show normalized $\Delta C_p$ as a function of temperature. (B) $T_m$ values for different GC content dsRNAs (blue) and their equivalent dsDNAs (red). Bars for each data point represent the width of the corresponding transition, which is larger for dsRNA since its melting transition is less cooperative than that of dsDNA.

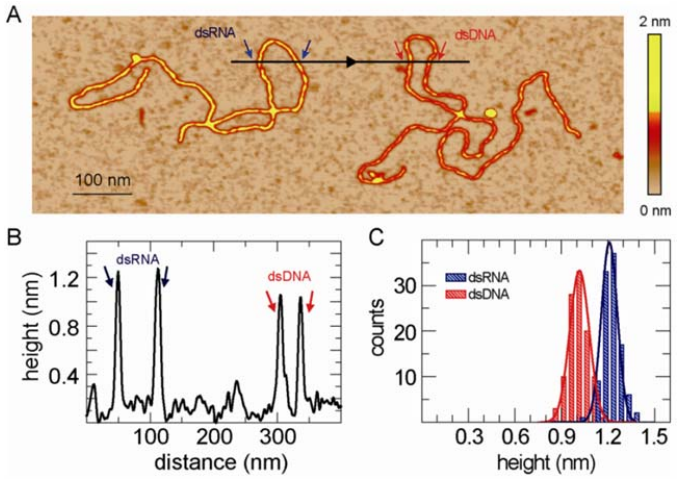


**Figure 3.** Atomic Force Microscopy structures of dsRNA and dsDNA. (A) High resolution AFM topographic image of two representative molecules deposited on the same mica surface. Color scale (from dark to bright) is 0-2 nm and was adjusted to highlight the larger height measured for dsRNA. (B) Height profile of the dsRNA and dsDNA molecules shown in (A) taken in the direction of the black arrow. (C) Height distribution of dsRNA and dsDNA molecules co-adsorbed over the same mica surface. Gaussian fits are included with mean values and standard deviations of 1.20 ± 0.06 nm and 1.00 ± 0.06 nm, respectively.

peaks[24], the most intense with a melting temperature ($T_m$) of 91°C. These same peaks are apparent within the less cooperative transition observed for dsRNA, whose global melting temperature is detected around 93°C, above that of dsDNA. The same relative behavior between dsRNA and dsDNA was maintained for sequences with different GC content. Specifically, we extended comparative $T_m$ measurements to dsRNA molecules with same 4-kbp length and GC densities ranging from 35% to 60% and to their sequence-equivalent dsDNA molecules. Results are shown in Fig. 2B: $T_m$ values increased with GC content for both kinds of molecules, on the one hand, and dsRNAs exhibited in all cases higher $T_m$ than their dsDNA counterparts, on the other.

**Single-molecule analysis at zero force**. Single molecules of both dsDNA and dsRNA are amenable to examination by Atomic Force Microscopy (AFM). This approach allows a direct measurement of the intrinsic contour length and relative diameter of the molecules on a one by one basis thus avoiding the constraints imposed by interhelical interactions which may alter the rise per base-pair[9,11,25-27]. Under appropriate conditions, dsDNA adheres to a mica surface weakly enough that dsDNA-mica interactions do not affect the chain statistics[28]. Molecules therefore adopt two-dimension equilibrium conformations that can be captured by AFM; from these molecule trajectories, the persistence length, *P*, can be measured (see below).

Standard methods to equilibrate DNA molecules on a mica substrate use $Mg^{+2}$ as a divalent cation[9,19,20,28]. However, this procedure failed to adsorb molecules of dsRNA due to their different intercalating stereochemistry on this nucleic acid. Pre-treatment of the mica surface with polylysine promoted adsorption of dsRNA, but molecules were kinetically trapped, as described elsewhere[16]. Other methods using spermidine, $CaCl_2$ and $MnCl_2$ were also explored but none of them resulted in either adsorption of dsRNA molecules ($CaCl_2$ and $MnCl_2$) or equilibration (spermidine). Notably, we found that the presence of $NiCl_2$ in the buffer at low nM concentrations allowed adsorption of both dsDNA and dsRNA molecules (see Experimental Section) granting access to the simultaneous comparison of their elastic properties. $Mg^{2+}$ and $Ni^{2+}$ cations are almost the same size but the affinity for base complexation relative to phosphate binding is higher for the latter[6,29]. The presence of a dislocation in the dsRNA bases moves part of the phosphate groups on each helix turn farther away from the mica surface than for the case of dsDNA bases, thus decreasing the adsorption forces between dsRNA and the mica surface with respect to the case of dsDNA. Our assays show that $Ni^{2+}$ provides the required affinity to bridge the negative phosphate groups in both dsRNA and dsDNA substrates with the negative mica surface in the absence of kinetic trapping effects.

Figure 3A shows an AFM image of two representative molecules of dsRNA and dsDNA co-adsorbed on the same mica surface. The mean contour length for dsRNA and dsDNA was 1.18 ± 0.05 μm (n=27) and 1.43 ± 0.05 μm (n=20), yielding a rise per base-pair of 0.29 ± 0.01 nm and 0.36 ± 0.01 nm, respectively. Similar values were obtained using $MgCl_2$ for dsDNA or polylysine for both dsDNA and dsRNA. These results are consistent with B-family conformations adopted by the dsDNA molecules (0.30-0.34 nm) and A-family conformations for dsRNA (0.27-0.30 nm)[6]. Co-adsorption of both kinds of molecules with the same base-pair sequence also allowed comparison of their heights (Fig. 3B), which are accurate with AFM within sub-Angstrom resolution. These measurements discriminated two types of transversal profiles, in agreement with B and A crystalline helices for which dislocation of the bases with respect to the helix axis produces different diameters[6,7]. DsRNA molecules are higher (1.20 ± 0.06 nm vs 1.00 ± 0.06 nm) than their DNA counterparts. DsDNA height was consis-

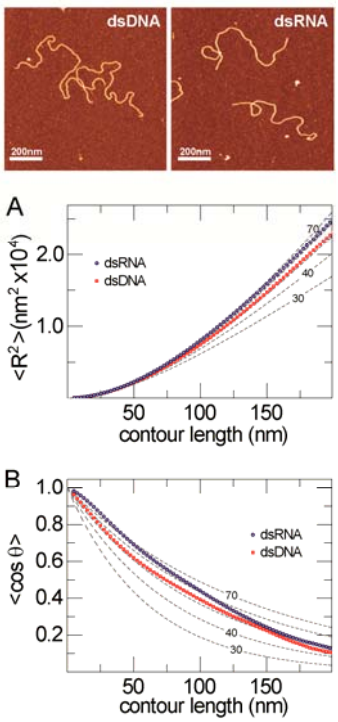


**Figure 4.** Atomic Force Microscopy analysis of the mechanical properties of dsRNA and dsDNA. Top, representative AFM images of dsDNA and dsRNA. Color scale from dark to bright is 0-2 nm. (A) and (B), plots of $\langle R^2 \rangle$ and $\langle cos\theta \rangle$ versus contour length spacing, $L$, of these dsRNA and dsDNA molecules equilibrated on a mica surface. dsDNA and dsRNA data follow the Worm-like chain (WLC) model, Eqs. 1 and 2, with persistence lengths of 51 ± 1 nm and 60 ± 1 nm, respectively. To guide the eye, WLC model data for $P$ = 30, 40, 50, 60, and 70 nm are included (dashed lines).

tently below its crystallographic value but in agreement with extensive measurements performed by AFM[30-32]. Our data allows a comparison between dsRNA and dsDNA because profiles are taken on the same image and therefore under identical conditions. Higher molecules showed perfect correlation with shorter contour lengths, a structural feature which allows a univocal identification of dsRNA vs dsDNA on the same mica surface. Figure 3C shows height distributions for dsRNA and dsDNA molecules, both reconstructed from AFM single-molecule measurements. Statistical populations are clearly separated, in agreement with early ensemble measurements of the rise per base-pair by crystallography[6,7]. We conclude from the experimental data in Fig. 3 that distinctive structural features of dsRNA and dsDNA are not only a result of ensemble averages but also of the individual substrates.

Next, we tested if the molecules were indeed equilibrated using $NiCl_2$, a prerequisite to determine $P$ from molecule trajectories. The trajectories were described as a chain of uncorrelated segments of a fixed length and the persistence length was calculated from averaging over hundreds of trajectories and discretized data points using the following equations:

$$\langle R^2_{s,\,s+L} \rangle = 4P(L + 2P(e^{-L/2P} - 1)), \quad [1]$$

$$\langle cos\theta_{s,\,s+L} \rangle = e^{-L/2P}, \quad [2]$$

where $L$ is the contour length spacing and $\langle R^2_{s,\,s+L} \rangle$ is the mean-square separation of points along the chain as a function of their contour length separation, $L$, or located at distances $s$ and $s+L$. Likewise, $\langle cos\theta_{s,\,s+L} \rangle$ is the mean angle between tangents at contour points located at distances $s$ and $s+L$. The average is computed over s and over all observed contours. As a first check, we measured $\langle R^2_{s,\,s+L} \rangle$ as a function of $L$ between points up to 200 nm. If the chain conformations are in fact equilibrated this function should follow Eq. 1. Indeed, we found that the data follow this prediction (Fig. 4A). Likewise, the tangent-tangent correlation for equilibrated molecules must fall with contour separation $L$ as indicated in Eq. 2. Figure 4B shows that this function is also followed. Note, however, that this distribution applies a more stringent test for equilibration and extensive averaging is needed at longer contour lengths to avoid deviations from theory. Fits in Fig. 4A and 4B yield values for the persistence length of dsDNA and dsRNA of 51 ± 1 nm and 60 ± 1 nm, respectively. These two tests confirm that the co-adsorption method using $NiCl_2$ produces contours reflecting equilibrium two-dimension chain conformations. Two additional independent measurements of $P$ for dsRNA at 20 and 100 mM NaCl (Fig. S1, Supporting Information) confirm a larger rigidity for dsRNA compared to dsDNA, in agreement with previous reports[9,16,33,34].

**Single-molecule analysis in the presence of force.** To investigate the effect of force (0.1 pN – 100 pN) on dsRNA, we used the OT technique, following the scheme described in the Experimental Section and depicted in the inset of Fig. 5A, in which a double stranded fiber is extended between two beads, one optically trapped and the other held by suction on a micropipette. With this method, we were able to stretch dsRNA molecules at high forces thus revealing that this substrate also overstretches in physiological conditions[35,36]. Its transition is less cooperative than in dsDNA, as can be observed by simple inspection of Fig. 5 (see also Fig. S2). DsRNA also exhibits important differences in the elastic behavior with respect to dsDNA as explained next.

*Elastic regimes and structural transitions.* Force-extension curves (stretch-relax cycles) for dsRNA and dsDNA are plotted in Figs. 5A, B and C for different salt concentrations. The main differences between the two molecules lie in the lengths of the entropic elasticity regime and the overstretching plateau. It is known that the end of the entropic elasticity regime is marked by the contour length of the molecule[8] and, in this regard, the length of the entropic plateau agrees with the above contour-length measurements in the absence of force by AFM (Table 1). Then, the force-extension measurements confirm that dsRNA is an intrinsically shorter molecule in the so-called A-form. Former experiments with dsDNA at high concentrations of ethanol and/or with high-GC content, both conditions promoting an A-type

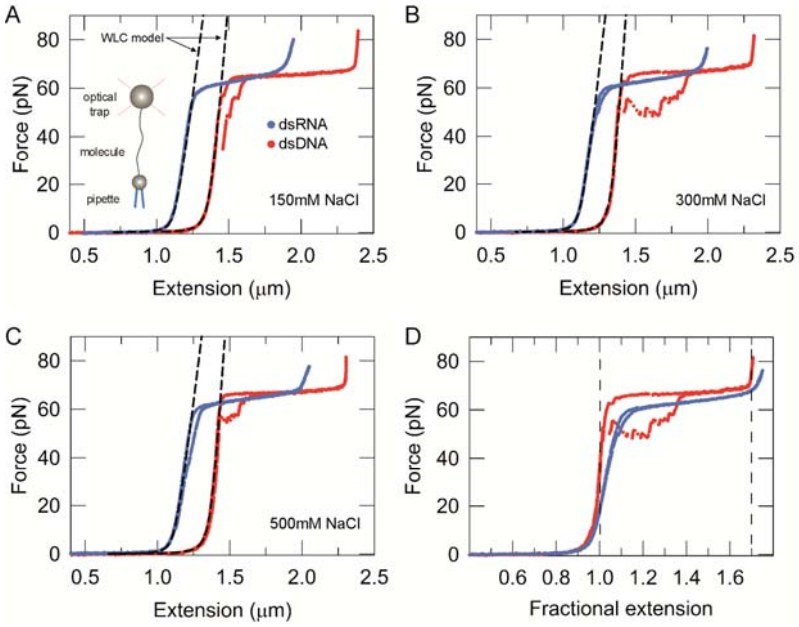


**Figure 5.** Force-extension characterization of dsRNA and dsDNA substrates using optical tweezers. Inset in (A), cartoon of a double-stranded molecule as placed in the OT (not to scale). The molecule is tethered between a bead (biotin-streptavidin linkage), held by suction on the top of a micropipette, and an optically trapped bead (Dig–α-Dig linkage). The molecule can be stretched by moving the micropipette through a piezo-actuator. (A-C) Force-extension curves at different salt concentrations. Blue and red dots correspond to data points of a dsRNA and a dsDNA molecule, respectively, with their corresponding fittings, black dashed curves, to the extensible WLC model (Eq. 3). The fits for these examples yielded values of (A) $L_0$ = 1.15 μm, $P$ = 67.7 nm and $S$ = 589 pN for dsRNA and $L_0$ = 1.39 μm, $P$ = 49.9 nm and $S$ = 1082 pN for dsDNA at 150 mM NaCl TE buffer; (B) $L_0$ = 1.14 μm, $P$ = 59.8 nm and $S$ = 632 pN for dsRNA and $L_0$ = 1.36 μm, $P$ = 48.5 nm and $S$ = 1280 pN for dsDNA at 300 mM NaCl; and (C) $L_0$ = 1.14 μm, $P$ = 57.7 nm and $S$ = 615 pN for dsRNA and $L_0$ = 1.40 μm, $P$ = 44.5 nm and $S$ = 1379 pN for dsDNA at 500 mM NaCl. (D) Same as in B with extension axis of each substrate molecule normalized to its respective contour length. Dashed lines at fractional extensions 1.0 and 1.7 demarcate the elasticity regimes.

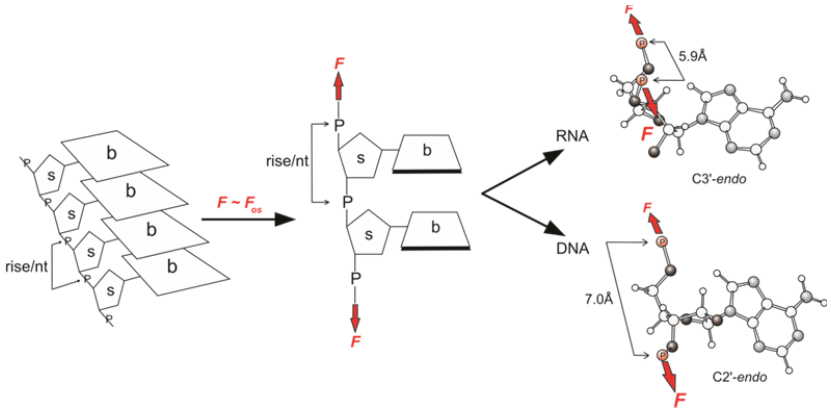


**Figure 6.** Schematic depiction of the elastic response of nucleic acids under force. Rise per nucleotide (rise/nt) depends on the stacking of bases (b) in the absence of stress. When force is applied at overstretching values ($F$~$F_{os}$), bases unstack and rise per nucleotide is restricted by the distance between phosphates linking adjacent sugar rings (s), which is of 5.9 Å in dsRNA, where sugar rings are in C3´-*endo* conformation, and of 7.0 Å in dsDNA, where they adopt the C2´-*endo* conformation[6].

base-stacking according to CD measurements, showed that these molecules extend in the entropic regime to a B-form contour length[9-11]. Therefore, the behavior of the so-called A-DNA is, by contrast with the dsRNA measurements shown in Figs. 5 and S2, strictly different from that of an intrinsic A-form molecule. The overstretching transition is also known to be related to the contour length. More in depth, dsDNA has been shown to extend to a 70% excess of its contour length during the overstretching transition[8], even for GC-rich DNAs and in low-humidity conditions[9,11]. DsRNA is consistent with this empiric rule considering its different contour length, as it overstretches to 1.7 times the length of an A-form nucleic acid.

It is remarkable, however, that the overstretched dsRNA molecules do not exhibit a total final length similar to that of dsDNA, which should occur provided that the distance between phosphates of the nearly unwound molecules, either from dsDNA or dsRNA, were the same under high tension. In this regard, Fig. 5D shows the general trend that has been observed within the population of dsDNA and dsRNA molecules stretched by OT: when the force-extension curves of dsDNA and dsRNA are normalized in the extension axis to their respective contour lengths and plotted together, the final extension of both molecules after the overstretching transition is approximately 1.7 in this representation. This fact reveals that the sugar-pucker conformation of the nucleotides plays a major role in the presence of force. It is known that A-type nucleotide helices adopt a so-called $C_3$'-endo conformation in which phosphate-phosphate distances in the polynucleotide chain is 0.59 nm. In contrast, B-type nucleotide helices, which adopt a $C_2$'-endo conformation, leave a distance between phosphates of 0.7 nm[6].

Figure 6 shows how the presence of force affects dissimilarly the final conformation of dsRNA and dsDNA upon overstretching due to their different stereochemical phosphate atom disposition. The fact that overstretched dsRNA molecules do not extend to a similar length to that of overstretched dsDNA in physiological conditions indicates that sugar-pucker conformations constraint phosphate bonds in very stringent orientations thus providing the polymer backbone with a very rigid structure which is not distorted at high stretching forces. As a consequence, dsRNA does not transition between the A and B forms in the presence of high force.

Another important difference is that overstretching forces in dsDNA are higher than in dsRNA for the same conditions. On comparing forces at half plateau length, dsRNA shows lower forces by approximately 2 pN (Table 1). This scenario was also found for dsDNA at low humidity, where the overstretching forces in alcohol were always lower by ~5 pN with respect to the same molecule in buffer[10,11]. The overstretching transition is also less cooperative for dsRNA than for dsDNA; it occurs within a broader force range for dsRNA (~10 pN at 500 nm/s pulling speed) than for dsDNA (~2 pN for the same velocity, as also reported elsewhere[35,36]), a fact which correlates with the distinct thermal behavior exhibited by these two substrates in the thermograms of Fig. 2. Specifically, dsRNA was shown to melt with reduced cooperativity with respect to its DNA counterpart. Therefore, the distinct cooperativity in the force-extension curves is consistent with distinct fraying in the overstretching transition, which might take place either by melting of a putative S-form double helix[35,36] or by melting of putative B and A-form cross links in the overstretched dsDNA and dsRNA, respectively[37-39]. Similar less cooperative overstretching transitions take place for dsDNA in alcohol[10,11] or at high temperature[40], although the plateaus are also accompanied by non-equilibrium rough force patterns which are absent in dsRNA.

With regards to the melting hysteresis area between stretch-relax paths[40,10], it is overall smaller for dsRNA

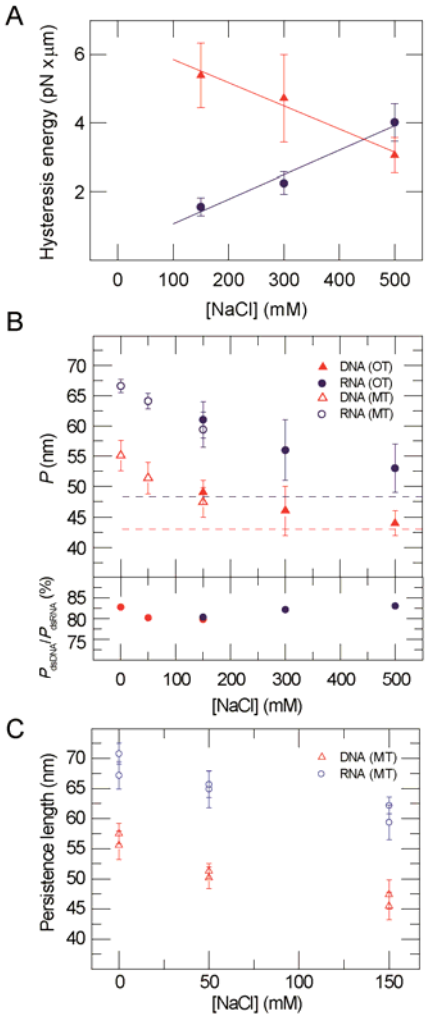


**Figure 7.** (A) Hysteresis area between stretch and release force-extension curves versus salt concentration for dsRNA (blue circles) and dsDNA (red triangles) molecules. Vertical bars represent standard error of at least 10 individual experiments (each with a different molecule) at each salt concentration. (Maximum hysteresis area is attained when the molecule relaxes as single-stranded and it is approximately 33 pN×μm for dsRNA and 45 pN×μm for dsDNA). (B, upper panel) Persistence length of dsRNA (blue) and dsDNA (red) versus salt concentration. Experiments were performed with OT (solid symbols) and MT (open symbols). Dashed lines mark the intrinsic persistence length (high-salt asymptotic limit). (B, lower panel) Persistence-length ratio of dsDNA to dsRNA. (C) Persistence length variation with salt concentration within a single molecule. The graph shows two experiments; in each one, a single molecule of either dsRNA (blue) or dsDNA (red) is examined at three ionic conditions.

than for control dsDNA molecules (see Figs. 5, A-C), thus indicating that the rate of strand annealing is faster for the former, as the stretch-release cycle is almost reversible at the used loading rate. A quantitative analysis of the hysteresis area is shown in Fig. 7A. Hysteresis area between stretch and relax paths, which is mild for both substrates at the ionic concentrations used, is related to force-induced melting and, in this regard, the results

**Table 1. Mechanical properties of dsRNA and dsDNA molecules of the same sequence*.**

| | | | $L_0$ (nm) | $P$ (nm) | $P_{el}$ (nm) | $S$ (pN) | $F_s$ (pN) |
|---|---|---|---|---|---|---|---|
| AFM | ($Ni^{2+}$) | dsRNA | 1180 (50) | 60 (1) | – | – | – |
| | | dsDNA | 1430 (50) | 51 (1) | – | – | – |
| MT | 0 mM $Na^+$ | dsRNA | 1130 (140) | 66.6 (1.1) | 18.6 | – | – |
| | | dsDNA | 1300 (100) | 55.1 (2.5) | 12.1 | – | – |
| | 50 mM $Na^+$ | dsRNA | 1060 (110) | 64.1 (1.3) | 16.1 | – | – |
| | | dsDNA | 1300 (100) | 51.4 (2.6) | 8.4 | – | – |
| | 150 mM $Na^+$ | dsRNA | 1150 (180) | 59.4 (2.9) | 11.4 | – | – |
| | | dsDNA | 1280 (160) | 47.4 (2.4) | 4.4 | – | – |
| OT | 150 mM $Na^+$ | dsRNA | 1149 (1) | 61 (3) | 13 | 500 (29) | 63.6 (2.0) |
| | | dsDNA | 1397 (3) | 49 (2) | 6 | 935 (121) | 65.6 (1.3) |
| | 300 mM $Na^+$ | dsRNA | 1145 (1) | 56 (5) | 8 | 632 (34) | 64.6 (1.8) |
| | | dsDNA | 1386 (3) | 46 (4) | 3 | 1165 (156) | 67.1 (1.1) |
| | 500 mM $Na^+$ | dsRNA | 1143 (1) | 53 (4) | 5 | 683 (63) | 65.9 (3.3) |
| | | dsDNA | 1391 (5) | 44 (2) | 1 | 1203 (51) | 67.0 (2.8) |

$L_0$, contour length; $P$, persistence length; $P_{el}$, electrostatic persistence length; $S$, stretch modulus; $F_s$, overstretching force at half transition. Standard error used (in brackets) except for the $F_s$ and MT data (standard deviation). Number of dsRNA sample molecules, n ≥ 11. *Fragment from the [30286, 34286] sequence of λ DNA (47.3% GC, 4.0 kbp, Fig. 1A).

from Fig. 7A are in agreement with the thermograms of Fig. 2: the melting stability of dsRNA is higher (higher melting temperature, lower force-induced mechanical hysteresis area) than that of dsDNA[41,42] at 150 mM [NaCl]. Interestingly, mean hysteresis area values are observed to increase with salt concentration for dsRNA, while the opposite trend is observed for dsDNA, in which melting hysteresis decreases with the increment of salt concentrations[10,33]. A cross-over point at around 450 mM monovalent salt concentration indicates that dsRNA and dsDNA show similar melting stability.

The presence of nicks in the molecules plays an important role in interpreting both Figs. 5 and 7A. Our construction methods for obtaining both dsRNA and dsDNA do not include nicks intentionally, as they involve the ligation of a double-stranded main molecule to two double-stranded multilabeled ends, with labeled nucleotides in both strands (see Experimental Section). However, prior to use in the optical tweezers we performed single-molecule MT rotation measurements in order to test if our molecules were torsionally constrained or had incorporated any occasional nicks during the preparation procedure, which is very likely to happen, especially in the case of dsRNA due to the labile nature of single-stranded intermediates. These measurements revealed that most of the dsRNA molecules were free to rotate, which means that most of them had nicks. This scenario perfectly correlates with what was found when both kinds of molecules were stretched in the optical tweezers, where 15% of the dsDNA molecules and less than 1% of the dsRNA molecules were found to overstretch as torsionally constrained molecules, at higher forces[21,39,43-45].

*Mechanical properties*. To adjust the entropic and intrinsic elasticity regimes of force-extension curves measured with OT we used a variation of the WLC model which takes into account that the molecules can be stretched beyond its contour length. The extensible WLC model in the so-called strong-stretching limit incorporates an elastic stretch modulus, $S$, as[46]:

$$z = L_0\left[1-\frac{1}{2}\left(\frac{k_BT}{FP}\right)^{1/2}+\frac{F}{S}\right] \qquad [3]$$

We used this expression to fit the force-extension curves in the range 1 – 40 pN. Examples of these fits are shown as black dashed lines in Figs. 5, A-C. Best fit of Eq. 3 to the data yielded a contour length, $L_0$, a persistence length, $P$, and a stretch modulus, $S$, for each dsRNA and dsDNA molecule which are summarized on Table 1. At 150 mM NaCl, for example, the mean rise per base-pair for dsRNA (dsDNA) is 0.29 ± 0.01 nm (0.35 ± 0.01 nm), $P$= 61 ± 3 nm (49 ± 2 nm) and $S$= 500 ± 29 pN (935 ± 121 pN). We observed that mean values of $L_0$ for dsRNA and dsDNA are consistent with A and B conformational families, respectively[6]. Likewise, $L_0$ and $P$ derived from these fittings for both kinds of molecules are very similar to the values previously measured by AFM.

Single molecules of dsRNA were difficult to capture at low salt concentration due to the different electrostatic behavior of dsRNA with respect to that of dsDNA. To determine the persistence-length behavior below 150 mM [NaCl], molecules were first captured at high salt concentrations; then, the buffer was gently replaced by that with the appropriate (lower) salt concentration. This experimental procedure was more easily followed in a MT setup since this technique allows tracking of more than one molecule at a time. Force-extension curves up

to 4 pN with MT (Fig. S3) concurrently provided a further check of the contour and persistence lengths determined at 150 mM [NaCl] against previous OT measurements. Persistence length results measured by MT are summarized on Table 1 and the complete set of results, from 0 to 500 mM [NaCl], are plotted in Fig. 7B, upper panel. *P* values for dsRNA are always larger than those for dsDNA at the same conditions and they decrease with the increment of salt concentration, as in dsDNA[33]. Data for dsDNA show consistency with former literature. Interestingly, the ratio of persistence lengths remained essentially constant with salt concentration, about 80% (Fig. 7B lower panel). Separating the electrostatic ($P_{el}$) and intrinsic ($P_0$) contributions to the overall persistence length ($P=P_0+P_{el}$, Table 1)[33] by taking $P_0$ as the asymptotic value at high salt (*Poisson-Boltzmann* theory for uniformly charged cylinders) in Fig. 7B (~48 nm, dsRNA, and ~43 nm, dsDNA), it is observed that both contributions are larger in dsRNA. Finally, Fig. 7C shows the persistence length variation with salt concentration within a single molecule. These experiments confirm that the decrease in *P* with salt concentration is not only a result of averages but also of the individual substrates.

OT measurements in the intrinsic elasticity regime further reveal that the stretch modulus of dsRNA increases with salt concentration, in agreement with the trend observed for dsDNA[33], but with *S* values much lower than those of dsDNA. It is worth noting that the *S* values from the fragment of λ-DNA used to prepare molecules in this study are slightly below those reported for the complete λ-DNA[33] or previously characterized high-GC content molecules[9] due to the lower GC content of the sample molecules used here (Fig. 1A). Contour lengths are also slightly larger than results from these references due to the weaker base-stacking exhibited by lower GC content DNA. Persistence length determinations near 0 mM [NaCl] may also be affected by the different buffering conditions used here with respect to previous studies[33].

## DISCUSSION

The mechanical properties and overstretching behavior of both dsRNA and dsDNA are deeply rooted on their distinct structures, and these in turn are related to their stereochemical identities. Specifically, the length of the entropic plateau in dsRNA complies with an A-form contour-length whereas in dsDNA this applies for the B-form contour-length. This low-force stretching behavior is in agreement with their different rise per base-pair[6,7]

With regards to the final extension of the individual molecules after the overstretching transition, it is of 1.7 times the A-form contour-length for dsRNA, and it is of 1.7 times that of the B-form for dsDNA. This high-force stretching behavior is in agreement with the different distance between phosphates in the $C_3$'-endo and the $C_2$'-endo sugar-pucker modes which are characteristic of the RNA and DNA polynucleotide chains, respectively[6]. Although the so-called A-DNA presents a qualitatively similar CD spectrum and its mechanical properties resemble more those of dsRNA[10], it is a major conclusion of this work that the A form in dsRNA is an intrinsic structure of the molecule in contrast to what happens to dsDNA, where the A-like polymer however extends like a B-form molecule even in the presence of low humidity conditions[11] or for dsDNAs with high-GC content[9]. In this regard, former experiments showed that A-type base-stacking for dsDNA at low humidity coexists with condensation[11], a fact that suggested that a reduced rise per base-pair in dsDNA is a further consequence of the global stabilization of the DNA polymer induced by lateral chain interactions[9-11].

In light of these results, differences in bending and stretching rigidities and in the overstretching transition reveal a connection to these structural identities. Specifically, the absence of co-planarity (i.e. the presence of a non-zero so-called roll angle) in the stacking of the bases in dsRNA and the dislocation of the bases with respect to the axis diameter (i.e. the presence of a non-zero so-called slide displacement)[7] conform to a less optimal piling geometry between the bases which should lead to weaker base-stacking forces than in dsDNA, for which the roll angle and slide displacement are almost zero. A weaker base-stacking correspond to a smaller stretch modulus. Likewise, the lack of an optimal piling geometry is consistent with a less organized process of base unstacking in the presence of mechanical or heat stresses which should lead to less cooperative overstretching and melting transitions, respectively. The lower hysteresis area between stretch and relax paths in the force-extension curves of dsRNA with respect to dsDNA is also consistent with a higher melting temperature for dsRNA.

Finally, the fact that the distance between phosphates in dsRNA is shorter than in dsDNA makes negative charges along the sugar-phosphate backbone more proximate for the former hence increasing the polymer surface charge density. A higher negative charge density leads to a greater electrostatic self-repulsion between chain segments, what subsequently increases the electrostatic component of the persistence length of dsRNA with respect to that of dsDNA[47-51]. The presence of a slide displacement in the bases in dsRNA makes the polymer wider, as structurally determined in earlier studies[6] and measured here at the single-molecule level by AFM, thus resulting in a rod structure intrinsically less bendable than its DNA counterpart and subsequently increasing the intrinsic component of the persistence length of dsRNA with respect to dsDNA[47,48]. The combination of structural data with our mechanical analysis thus shows that the electrostatic and intrinsic components of the persistence length cooperate in making the bending rigidity of dsRNA larger than that of dsDNA.

The presence of the overstretching transition in dsRNA and the smaller hysteresis area of this substrate with respect to dsDNA at the same conditions indicate that, (1), an S-RNA structure can be proposed, paralleling the S-DNA conformation[35,36] and, (2), force-induced melting[37-39] is a possible mechanism provided that a rapid re-annealing after fraying from nicks takes place. In this latter regard, we speculate that the high tendency of RNA to form single-stranded secondary structures should compete against the dsRNA re-annealing upon relaxation. This competition should show as a larger hysteresis

area in the force-extension curves of dsRNA with respect to those of dsDNA which did not take place in our experiments. Likewise, the presence of more than one nick, which is more probable in dsRNA than in dsDNA due to the lower ligation efficiency of the former (see Experimental Section and Results), should lead to the loss of ssRNA fragments from some molecules. We never observed a partial or total ssRNA relaxation curve after the overstretching. In contrast, RNA molecules repeatedly stretched as a double-stranded arrangement in subsequent extension cycles (stretching force-extension paths corresponding to different cycles of the same molecule always superimposed one another). This evidence is interpreted here as a longer prevalence of the S-RNA in the corresponding overstretching transition over the force-induced molten allomorphs for dsRNA, in agreement with a scenario in which the generation of ssRNA or ssDNA from nicks or free ends is not necessarily concomitant with overstretching but a consequence of both the resulting tension and/or the denaturing environmental conditions[45,52,53].

## CONCLUSIONS

Long dsRNA molecules and their dsDNA counterparts with equivalent sequence have been stretched for their complete mechanical and structural characterization. A and B-form patterns for dsRNA and dsDNA, respectively, have been checked by CD confirming their distinctive base-stacking conformations and DSC experiments have shown that dsRNA melts in a less cooperative fashion than dsDNA. Then, single-molecule microscopy has been performed by AFM. The coadsorption method used here has afforded a single-molecule direct comparison of both molecules, not only regarding measurements of their contour and persistence lengths, but also of their height over the same mica surface. Force-extension curves have shown a lower resilience of dsRNA with respect to dsDNA since the former presents a lower stretch modulus and its overstretching transition takes place at a lower force and in a less cooperative fashion than the latter. DsRNA shows a larger bending rigidity than dsDNA as a result of the larger electrostatic and intrinsic contributions to the overall persistence length in dsRNA. These measurements have been discussed to be related to the differences in geometric parameters and stereochemistry characterizing A and B-form nucleic acids.

## ASSOCIATED CONTENT

**Supporting Information**. Additional AFM, OT and MT experiments. This material is available free of charge via the Internet at http://pubs.acs.org.

## AUTHOR INFORMATION

### Corresponding Authors

* ricardo.arias@imdea.org
* fernando.moreno@cnb.csic.es

## ACKNOWLEDGMENT

This work was supported by grants from the Spanish Ministry of Science and Innovation (BFU2011-29038 and BFU2010-15703) and the Comunidad de Madrid (S2009/MAT/1507). J.R. A.-G. acknowledges a Ramón y Cajal contract from the Spanish Ministry of Science and Innovation (RYC-2007-01765). Work in the F.M.-H. laboratory was supported by a Starting Grant from the European Research Council (no. 206117) and a grant from the Spanish Ministry of Science and Innovation (FIS2011-24638). The authors thank M.S. Dillingham for kindly providing the pSP73-JY0 plasmid, M. Menendez for access to a spectropolarimeter, A. Monserrate for polylysine-AFM control experiments and B. Ibarra for fruitful discussions.

## ABBREVIATIONS

Ds, double-stranded; CD, Circular dichroism; DSC, Differential Scanning Calorimetry; GC, Guanine-Cytosine; AFM, Atomic Force Microscopy; WLC, worm-like chain; OT, Optical Tweezers; MT, Magnetic Tweezers.

## REFERENCES

(1) Fire, A.; Xu, S.; Montgomery, M. K.; Kostas, S. A.; Driver, S. E.; Mello, C. C. *Nature* **1998**, *391*, 806-11.
(2) Montgomery, M. K.; Xu, S.; Fire, A. *Proc Natl Acad Sci USA* **1998**, *95*, 15502-7.
(3) Timmons, L.; Fire, A. *Nature* **1998**, *395*, 854.
(4) Guo, *P. Nat Nanotechnol* **2010**, *5*, 833-42.
(5) Bumcrot, D.; Manoharan, M.; Koteliansky, V.; Sah, D. W. *Nat Chem Biol* **2006**, *2*, 711-9.
(6) Saenger, W. *Principles of nucleic acid structure*; 2nd ed.; Springer-Verlag: NY, **1984**.
(7) Calladine, C. R.; Drew, H. R.; Luise, B. F.; Travers, A. A. *Understanding DNA. The molecule and how it works*; Third ed.; Elsevier. Academic Press, **2004**.
(8) Bustamante, C.; Bryant, Z.; Smith, S. B. *Nature* **2003**, *421*, 423-7.
(9) Hormeno, S.; Ibarra, B.; Carrascosa, J. L.; Valpuesta, J. M.; Moreno-Herrero, F.; Arias-Gonzalez, J. R. *Biophys J* **2011**, *100*, 1996-2005.
(10) Hormeno, S.; Ibarra, B.; Valpuesta, J. M.; Carrascosa, J. L.; Arias-Gonzalez, J.R. *Biopolymers* **2012**, *97*, 199-208.
(11) Hormeno, S.; Moreno-Herrero, F.; Ibarra, B.; Carrascosa, J. L.; Valpuesta, J. M.; Arias-Gonzalez, J. R. *Biophys J* **2011**, *100*, 2006-15.
(12) Seidel, R.; Dekker, C. *Curr Opin Struct Biol* **2007**, *17*, 80-6.
(13) Tinoco, I.; Chen, G.; Qu, X. *Cold Spring Harb Perspect Biol* **2010**, *2*, a003624.
(14) Arias-González, J.R. *PLoS ONE* **2012** 7(8): e42272.
(15) Dekker, N. H.; Abels, J. A.; Veenhuizen, P. T.; Bruinink, M. M.; Dekker, C. *Nucleic Acids Res* **2004**, *32*, e140.
(16) Abels, J. A.; Moreno-Herrero, F.; van der Heijden, T.; Dekker, C.; Dekker, N. H. *Biophys J* **2005**, *88*, 2737-44.
(17) Hormeno, S.; Arias-Gonzalez, J. R. *Biol Cell* **2006**, *98*, 679-95.
(18) Horcas, I.; Fernandez, R.; Gomez-Rodriguez, J. M.; Colchero, J.; Gomez-Herrero, J.; Baro, A. M. *Rev Sci Instrum* **2007**, *78*, 013705.
(19) Moreno-Herrero, F.; Seidel, R.; Johnson, S. M.; Fire, A.; Dekker, N. H. *Nucleic Acids Res* **2006**, *34*, 3057-66.
(20) Wiggins, P. A.; van der Heijden, T.; Moreno-Herrero, F.; Spakowitz, A.; Phillips, R.; Widom, J.; Dekker, C.; Nelson, P. C. *Nat Nanotechnol* **2006**, *1*, 137-41.
(21) Smith, S. B.; Cui, Y.; Bustamante, C. *Methods Enzymol* **2003**, *361*, 134-62.
(22) Ivanov, V. I.; Minchenkova, L. E.; Schyolkina, A. K.; Poletayev, A. I. *Biopolymers* **1973**, *12*, 89-110.
(23) Brahms, J.; Mommaerts, W. F. *J Mol Biol* **1964**, *10*, 73-88.
(24) Cantor, C. R.; Schimmel, P. R. *Biophys Chem*; W.H. Freeman and Company: New York, **1980**.

(25) Herbeck, R.; Yu, T. J.; Peticolas, W. L. *Biochemistry* **1976**, *15*, 2656-60.
(26) Nishimura, Y.; Torigoe, C.; Tsuboi, M. *Biopolymers* **1985**, *24*, 1841-1844.
(27) Mazur, A. K. *J Chem Theory Comput* **2005**, *1*, 325-336.
(28) Rivetti, C.; Guthold, M.; Bustamante, C. *J Mol Biol* **1996**, *264*, 919-32.
(29) Subirana, J. A.; Soler-Lopez, M. *Annu Rev Biophys Biomol Struct* **2003**, *32*, 27–45.
(30) Moreno-Herrero, F.; Colchero, J.; Baro, A. M. *Ultramicroscopy* **2003**, *96*, 167-74.
(31) Lyubchenko, Y. L.; Oden, P. I.; Lampner, D.; Lindsay, S. M.; Dunker, K. A. *Nucleic Acids Res* **1993**, *21*, 1117-23.
(32) Thomson, N. H.; Kasas, S.; Smith; Hansma, H. G.; Hansma, P. K. *Langmuir* **1996**, *12*, 5905-5908.
(33) Baumann, C. G.; Smith, S. B.; Bloomfield, V. A.; Bustamante, C. *Proc Natl Acad Sci USA* **1997**, *94*, 6185-90.
(34) Hagerman, P. J. *Annu Rev Biophys Biomol Struct* **1997**, *26*, 139-56.
(35) Smith, S. B.; Cui, Y.; Bustamante, C. *Science* **1996**, *271*, 795-9.
(36) Cluzel, P.; Lebrun, A.; Heller, C.; Lavery, R.; Viovy, J. L.; Chatenay, D.; Caron, F. *Science* **1996**, *271*, 792-4.
(37) Williams, M. C.; Wenner, J. R.; Rouzina, I.; Bloomfield, V. A. *Biophys J* **2001**, *80*, 1932-9.
(38) Wenner, J. R.; Williams, M. C.; Rouzina, I.; Bloomfield, V. A. *Biophys J* **2002**, *82*, 3160-9.
(39) van Mameren, J.; Gross, P.; Farge, G.; Hooijman, P.; Modesti, M.; Falkenberg, M.; Wuite, G. J.; Peterman, E. J. *Proc Natl Acad Sci USA* **2009**, *106*, 18231-6.
(40) Mao, H.; Arias-Gonzalez, J. R.; Smith, S. B.; Tinoco, I., Jr.; Bustamante, C. *Biophys J* **2005**, *89*, 1308-16.
(41) Searle, M. S.; Williams, D. H. *Nucleic Acids Res* **1993**, *21*, 2051-6.
(42) Sugimoto, N.; Nakano, S.; Katoh, M.; Matsumura, A.; Nakamuta, H.; Ohmichi, T.; Yoneyama, M.; Sasaki, M. *Biochemistry* **1995**, *34*, 11211-6.
(43) Leger, J.-F.; Romano, G.; Sarkar, A.; Robert, J.; Bourdieu, L.; Chatenay, D.; Marko, J.F. *Phys. Rev. Lett.* **1999**, *83*, 1066.
(44) Clausen-Schaumann, H; Rief, M; Tolksdorf, C; Gaub, H.E. *Biophys J.* **2000**, *78*(4), 1997-2007.
(45) Paik, D. H.; Perkins, T. T. *J Am Chem Soc* **2011**, *133*, 3219-21.
(46) Odijk, T. *Macromolecules* **1995**, *28*, 7016-8.
(47) Li, L.; Pabit, S. A.; Meisburger, S. P.; Pollack, L. *Phys Rev Lett* **2011**, *106*, 108101.
(48) Bustamante, C.; Smith, S. B.; Liphardt, J.; Smith, D. *Curr Opin Struct Biol* **2000**, *10*, 279-85.
(49) Savelyev, A. *Phys Chem Chem Phys* **2012**, *14*, 2250-2254.
(50) Cherstvy, A. G. *Phys Chem Chem Phys* **2011**, *13*, 9942-9968.
(51) Savelyev, A.; Materese, C. K.; Papoian, G. A. *J Am Chem Soc* **2011**, *133*, 19290-19293.
(52) Whitelam, S.; Pronk, S.; Geissler, P. L. *Biophys J* **2008**, *94*, 2452-69.
(53) Fu, H.; Chen, H.; Marko, J.F.; Yan, J. *Nucleic Acids Res.* **2010**, *38*, 5594-5600.

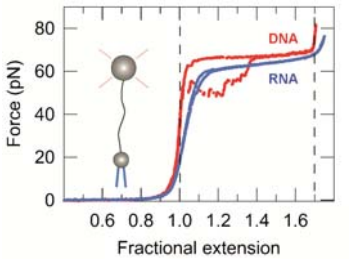
80
60
40
20
0
Force (pN)
DNA
RNA
0.6 0.8 1.0 1.2 1.4 1.6
Fractional extension